BRIEF COMMUNICATION   OPEN

Check for updates

AAV dose-dependent transduction efficiency in retinal ganglion cells and functional efficacy of optogenetic vision restoration

Qi Lu [1], Anna Wright[1] and Zhuo-Hua Pan [1]✉

Optogenetics is a promising approach for restoring vision to the blind after photoreceptor degeneration. The ability to restore vision through AAV-mediated delivery of light-sensitive proteins, especially channelrhodopsins, into retinal ganglion cells has been extensively demonstrated in animal models. For clinical application, knowledge of viral dose-dependent functional efficacy is desired. In this study, using a triple-knockout blind mouse model and a highly light-sensitive channelrhodopsin variant, we evaluated viral dose-dependent vision restoration through retinal ganglion cell expression by using optomotor behavioral assays. Our results show that both the restored light sensitivity and visual acuity reached peak levels at a medial viral dose of 10^8 vg. With increasing dose, transduction efficiency continued to increase while protein expression peaked at the dose of ~10^9 vg and declined at higher doses. Also, a significant increase in retinal gliosis and inflammatory responses started at the dose of ~10^9 vg, and a marked increase was observed at the dose of ~10^{10}. These results provide valuable insights into viral dose design for clinical studies.

INTRODUCTION
The death of photoreceptor cells in retinal degenerative diseases, such as retinitis pigmentosa and age-related macular degeneration, often leads to vision impairment or complete blindness [1, 2]. Optogenetics is a promising approach for restoring vision to the blind through the ectopic expression of genetically encoded light sensors (GELSs) in inner retinal neurons for imparting light sensitivity to the retina. Since the first proof of concept study using ChR2 [3], the optogenetic restoration of vision has been extensively demonstrated using a variety of optogenetic tools, particularly microbial channelrhodopsins (ChRs), in animal models [4–7]. Multiple clinical trials using ChR-based tools have been initiated since 2016, with partial restoration of vision reported [8]. Adeno-associated virus (AAV) vectors have been the leading platform of gene delivery for retinal gene therapy both in preclinical animal studies and human clinical trials [6, 7, 9].

The most commonly employed strategy for optogenetic vision restoration is to express a GELS in retinal ganglion cells (RGCs) [3, 10–18]. Other strategies include targeting ON bipolar cells or surviving cone photoreceptors [19–21]. RGC expression offers several major advantages. First, viral-mediated delivery of transgenes to RGCs can be achieved through intravitreal administration, a less-invasive and safer procedure than other delivery routes. Also, transgenes can be efficiently expressed in RGCs with ubiquitous promoters, such as the CMV immediate enhancer/β-actin (CAG) promoter. Furthermore, while photoreceptor cell death triggers retinal remodeling [22], RGCs are more resilient to retinal remodeling [23, 24]. Therefore, RGC targeting has been considered a last resort for optogenetic therapy at late stages of retinal degeneration.

A major hurdle of using ChR2 in particular and ChRs in general for vision restoration is their low light sensitivity [3]. We recently developed a highly light-sensitive ChR, CoChR-3M [16], through mutagenesis of a recently reported and more potent ChR variant from *Chloromonas oogama* (CoChR) [25]. AAV-mediated expression of CoChR-3M in RGCs enabled restoration of functional vision under ambient light conditions in a triple knock-out (TKO) blind mouse line, $Opn4^{-/-}$ $Gnat1^{-/-}$ $Cnga3^{-/-}$ [16]. The use of TKO mice takes advantage of their lack of optomotor response (OMR), pupillary constriction, and apparent photoreceptor cell death, which allows the optogenetically restored visual function to be quantitatively assessed with optomotor behavioral testing [26, 27].

However, the development of retinal gene therapy faces significant challenges in the form of immune responses against AAV and/or transgene-overexpression-caused stress or toxicity [28, 29]. Immune responses and associated adverse reactions are all viral dose-dependent. Therefore, identifying an optimal dose range with maximal efficacy and balanced safety is critical to the success of clinical trials. Notably, although optogenetic vision restoration by expressing ChRs in RGCs has been extensively validated in animal models, the relationship between viral dose and functional efficacy has not yet been systematically studied. In this study, we investigated the viral dose-dependent transduction efficiency in RGCs and the functional efficacy of CoChR3M-mediated vision restoration in TKO mice.

MATERIALS AND METHODS
Animals, viral vectors, and viral vector injection
TKO mice (B6129: $Opn4^{-/-}$ $Gnat1^{-/-}$ $Cnga3^{-/-}$) lack a rod-specific transducing unit, a cone photoreceptor-specific cyclic nucleotide channel

---

[1]Department of Ophthalmology, Visual and Anatomical Sciences, Wayne State University School of Medicine, Detroit, MI, USA. ✉email: zhpan@med.wayne.edu

Table 1. The mouse groups, viral doses, and animal numbers.

Mouse strain	Viral dose	Animals
TKO	1.5×10^7 vg	4
TKO	3.8×10^7 vg	5
TKO	7.5×10^7 vg	5
TKO	1.5×10^8 vg	5
TKO	7.5×10^8 vg	6
TKO	1.5×10^9 vg	6
TKO	7.5×10^9 vg	5
TKO	1.5×10^{10} vg	5
C57BL/6J	Not injected	5

subunit, and melanopsin [27]. The TKO mice were bred in-house whilst C57BL/6J mice were purchased from the Jackson Laboratory. Mice of both sexes were included in the experiments. Animals were housed under a standard 12 h/12 h light/dark cycle. All animal experiments and procedures were approved by the Institutional Animal Care and Use Committee of Wayne State University and were performed in accordance with the NIH Guide for the Care and Use of Laboratory Animals.

The viral vector used in this study has been previously reported [16]. The viral cassette contained the transgene of a triple mutant CoChR, CoChR-3M, fused in frame to GFP (CoChR-3M-GFP) and driven by the CAG promoter, the woodchuck hepatitis virus posttranscriptional regulatory element (WPRE), and the human growth hormone polyadenylation sequence (hGHpA). Viral vectors were packaged into the AAV2.7m8-Y444F capsid variant and affinity purified (Virovek, Hayward, CA, USA). This capsid variant was chosen due to its improved transduction efficiency in mice and non-human primates [26, 30, 31].

TKO mice of both sexes were injected intravitreally with viral vectors at the ages of 1–4 months. Briefly, each animal was anesthetized with an intraperitoneal injection of a mixture of 100 mg kg^{-1} ketamine and 12 mg kg^{-1} xylazine. Then, viral vectors diluted in saline to the desired dose with a volume of 1.5 μL were intravitreally injected into both eyes. The injection was performed using a programmable Nanoliter Injector (Drummond Scientific Company, Broomall, PA, USA) with glass micropipettes. C57BL/6J mice served as normal-sighted controls. The resource equation method was used to determine the sample size. Table 1 presents the animal groups and numbers. No animals were excluded from the analysis. Since the outcome of the treatment was not found to be animal age- or sex-dependent [16, 26], the method of animal randomization was not used. Investigators were not blinded to the animal group allocation during the experiment and/or when assessing the outcome. Behavioral tests were performed 1–2 months after the virus injection. Animals were euthanized by CO$_2$ asphyxiation, followed by decapitation for immunostaining and Western blot analysis.

Optomotor response (OMR) assays
The lack of OMR in TKO mice has been previously reported [26, 32]. Therefore, optomotor tests in TKO mice were not performed before AAV injection. A homemade optomotor system equipped with a video camera (iSight, Apple Inc) was used to measure the light sensitivity of the optogenetically treated TKO mice [26]. Illumination is provided by blue LEDs with peak emission at 470 nm, which is near the wavelength of CoChR-3M peak sensitivity. Light intensity is controlled by a digital power supply. OMR was tested using a rotation drum at a grating frequency of 0.042 cycle/degree for both clockwise and counterclockwise directions. Light sensitivity was defined as the lowest light intensity in either of the directions that was required to elicit OMR. The light sensitivity of C57BL/6J mice could not be measured because normal-sighted mice have greater light sensitivity than does the camera.

Visual acuity was measured using OptoDrum (StriaTech GmbH, Tübingen, Germany), an automatic virtual system [33]. The system is composed of four enclosed LCD monitors with an elevated animal platform in the center. The monitors display a grating stimulation that forms a virtual grating cylinder centered on the head of the animal. The light intensity of OptoDrum is fixed and is ~30 μW/cm^2 at the center of the platform. The grating stimulation was presented at a contrast of 100% with rotation speed of 12 degrees/second. Presentation of the grating stimulation, change of spatial frequency, and detection of the animal's head tracking were all executed algorithmically by the system. Since the most sensitive spatial frequency for the ChR-restored vision is at 0.042 cycle/degree [16], the test of head tracking started at the spatial frequency of 0.042 cycle/degree. Animals that failed at 0.042 cycle/degrees were recorded as zero visual acuity. Visual acuity was defined as the highest grating frequency that elicited OMR.

Immunostaining for assessing RGC density and retinal gliosis and inflammation
Enucleated eyes were fixed with 4% paraformaldehyde in 0.1 M phosphate buffer (PB) at room temperature for 20 minutes after removing the cornea and lens. Fluorescence expression was examined in flat-mounted retinas and retinal vertical sections. The expression of CoChR in RGCs was examined by co-labeling with goat anti-GFP antibody (1:1000; NB100-1770, Novus Biologicals, Centennial, CO, USA) and rabbit anti-RBPMS antibody (1:1000; ABN1362, MilliporeSigma, Temecula, CA, USA). Rabbit antibodies against glial fibrillary acidic protein (GFAP) (1:5000; G9269; Sigma-Aldrich, St. Louis, MO, USA) and ionized calcium-binding adapter molecule 1 (Iba1) (1:1000; AB178846; Abcam, Waltham, MA, USA) were used to assess gliosis and inflammatory responses, respectively. The secondary antibodies were conjugated to Alexa 488 (1:600) or Alexa 555 (1:600; Thermo Fisher Scientific, Waltham, MA, USA). Nuclei of retinal cells were stained with 4',6-diamidino-2- phenylindole (DAPI) (5 μM; Sigma-Aldrich).

The density of RGCs and of CoChR-3M-GFP-expressing RGCs was measured by assessing RBPMS-labeled and dual GFP/RBPMS-labeled cells, respectively. 3D Z-stack fluorescence images of retinal ganglion cell layers in retinal whole mounts were captured using the Zeiss Apotome 2 Optical Photomicroscope (Carl Zeiss AG, Oberkochen, Germany). Images were taken in eight evenly distributed locations in the middle regions of each retina ~1.0 mm from the optic disc. In each location, images of 10–15 planes in the ganglion cell layer at an interval of 1 μm were captured with the optimal exposure time using a 20x objective. The brightness and contrast were adjusted. All quantifications of cell density were performed using the ZEN software (Carl Zeiss AG). Cell numbers were manually counted with 'Points tools-events' in an 0.15 mm^2 area of the original Carl Zeiss Image file.

Immunostaining for assessing retinal gliosis and inflammation was performed in vertical retinal slices. Images were captured using a 40x objective. To enable quantitative comparison of GFAP immunoreactivity, the images were captured with the same exposure time (100 ms). GFAP fluorescent intensity was measured using the ZEN software, covering the area from inner nuclear layer to ganglion cell layer. Iba1 positive cells were counted from each image (224 μm in length). Both GFAP and Iba1 data were averaged from 12 images captured from six retinal slices, with two images from each slice.

Western blot analysis
Retinal tissue was lysed by sonication in RIPA buffer (89901, Thermo Fisher Scientific) with a 1% protease inhibitor cocktail (P8340, Sigma-Aldrich), and then centrifuged to remove debris. After quantification of total protein with the Pierce™ BCA Protein Assay Kit (23225, Thermo Fisher Scientific), the protein lysates were adjusted to 1 μg/μl, mixed with 2x Laemmli sample buffer (S3401, Sigma-Aldrich), and boiled for 10 min. Total protein samples (20 μg) were run on a 10% SDS-PAGE gel in Tris glycine-SDS buffer (LC2675, Thermo Fisher Scientific) for one hour at 100 V. The proteins were then transferred to a nitrocellulose membrane at 4 °C for 2 h. After blocking with 25% ChemiBlocker (MilliporeSigma) in 1x Tris-buffered saline containing 0.1% Tween 20 (TBST) for 1 h at 4 °C, the membrane was immunostained with the rabbit anti-GFP primary antibody (1:1000; A11122, Life Technologies, CA, USA) and rabbit anti-β-actin primary antibody (1:1000; PA5-72633, Life Technologies) in TBST overnight at 4 °C. The next day, the membrane was washed with 1X TBST three times and then incubated with the goat anti-rabbit horseradish peroxidase secondary antibody (1:2000, W4011, Promega, Madison, WI, USA) diluted in TBST with 25% ChemiBlocker at room temperature for 1 h. The membrane was washed with 1x TBST three times. Then the membrane is immersed in 5 ml freshly made ECL mixture for 2 min. Images of the membrane were captured with an Azure Biosystems Western Blot Imaging System for semi-quantification. ECL fluorescence bands were visualized and analyzed using a FluorChem System (Proteinsimple, San Jose, CA, USA). Fluorescence intensity was analyzed with the Image J software (NIH, US).
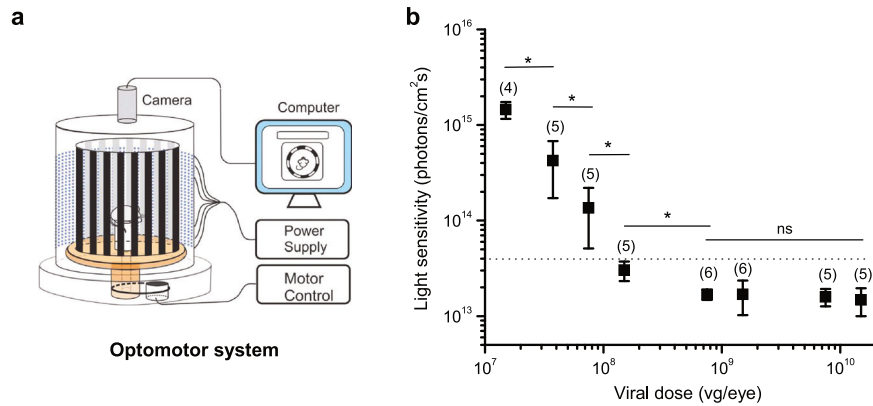
a

Optomotor system

b

Fig. 1 Dose-dependent light sensitivity of CoChR-3M-treated TKO mice, determined by OMR assay. a Diagram of the homemade optomotor system that was used for measuring light sensitivity. **b** The relationship of light sensitivity and viral vector dose. Light sensitivity was defined as the lowest light intensity that evoked OMR at the grating frequency of 0.042 cycle/degree. Data are presented as means ± SD ($n = 4$–6 mice in each group). Asterisk (*) indicates the values between the groups are significantly different ($p < 0.05$; one-way ANOVA). Light intensity values among the groups with viral dose $\geq 7.5 \times 10^8$ vg/eye are not significantly different (ns) ($p > 0.05$; one-way ANOVA). The dashed line indicates the estimated light intensity of the OptoDrum.
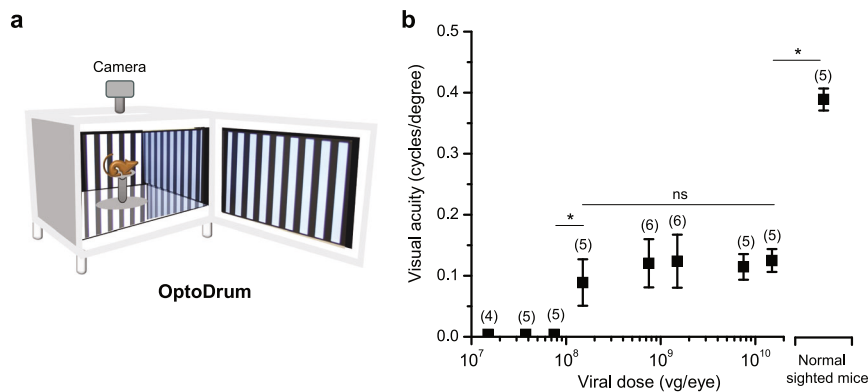
a

OptoDrum

b

Fig. 2 Dose-dependent visual acuity of CoChR-3M-treated TKO mice, determined by OMR assay. a The OptoDrum system (StriaTech GmbH, Tübingen, Germany) that was used for measuring visual acuity. **b** The relationship of visual acuity and viral vector dose. Visual acuity was determined as the highest grating frequency at 100% contrast that evoked OMR. Data are presented as means ± SD ($n = 4$–6 mice in each group). Asterisk (*) indicates the values between the groups are significantly different ($p < 0.05$; one-way ANOVA). Visual acuity values among the groups with viral dose $\geq 1.5 \times 10^8$ vg/eye are not significantly different (ns) ($p > 0.05$; one-way ANOVA).

Statistical analysis

Statistical analysis of all data was performed using the Origin program (OriginLab, Northampton, MA, USA). All data are presented as mean ± standard deviation. P values < 0.05 were considered statistically significant. All statistical tests and parameters are described in the figure legends.

RESULTS

Viral dose-dependent functional efficacy

Viral vectors were injected intravitreally in TKO mice at doses ranging from 1.5×10^7 vg/eye to 1.5×10^{10} vg/eye. Visual functions were assessed by optomotor behavioral assays. We first examined the dose-dependent light sensitivity, with light sensitivity defined as the lowest light intensity required to elicit OMR. The measurement was performed using a homemade optomotor system that allows altering the stimulus illumination (Fig. 1a) [26]. The relationship between viral dose (vg/eye) and light sensitivity was measured (Fig. 1b). The threshold light intensity decreased rapidly by about 50-fold, from 1.5×10^{15} ($\pm 3.2 \times 10^{14}$; mean ± SD; $n = 4$) to 3.0×10^{13} ($\pm 7.0 \times 10^{12}$; $n = 5$) photons/cm^{2}s, as the viral dose increased from 1.5×10^7 to 1.5×10^8 vg/eye. As viral dose increased from 1.5×10^8 to 7.5×10^8 vg/eye, the threshold light intensity decreased about two-fold to 1.7×10^{13} ($\pm 2.1 \times 10^{12}$; $n = 6$) photons/cm^{2}s. With further dose increase, the light

sensitivity approached a plateau; at the highest dose tested, 1.5×10^{10} vg/eye, the threshold light intensity was only slightly lower ($1.5 \times 10^{13} \pm 4.8 \times 10^{12}$; $n = 5$). Threshold light intensities for doses $\geq 7.5 \times 10^8$ vg/eye were not statistically different ($p > 0.05$; one-way ANOVA).

We next examined the restored visual acuity. Visual acuity was measured using OptoDrum (Fig. 2a), an automatic virtual optomotor system [33]. The relationship between the viral dose and visual acuity was obtained (Fig. 2b). OMR failed to be observed in mice injected with viral doses lower than 1.5×10^8 vg/eye. In contrast, OMR was observed in all mice injected with viral doses at 1.5×10^8 vg/eye and higher. The visual acuity was 0.089 ± 0.038 cycle/degree (mean ± SD; $n = 5$) at the dose of 1.5×10^8 vg/eye and reached 0.11–0.13 cycle/degree at higher doses. However, the visual acuity among mice receiving those higher doses was not statistically different ($p > 0.05$; one-way ANOVA). As a control, the visual acuity for normal sighted mice (C57BL/6 J) was 0.39 ± 0.018 cycle/degree (mean ± SD; $n = 5$), which was significantly higher than the treated groups ($p < 0.05$; one-way ANOVA).

Viral-dose-dependent transduction efficiency in RGCs

The viral dose-dependent expression was examined in vertical retinal slices and retinal whole mounts (Fig. 3a, b), respectively,
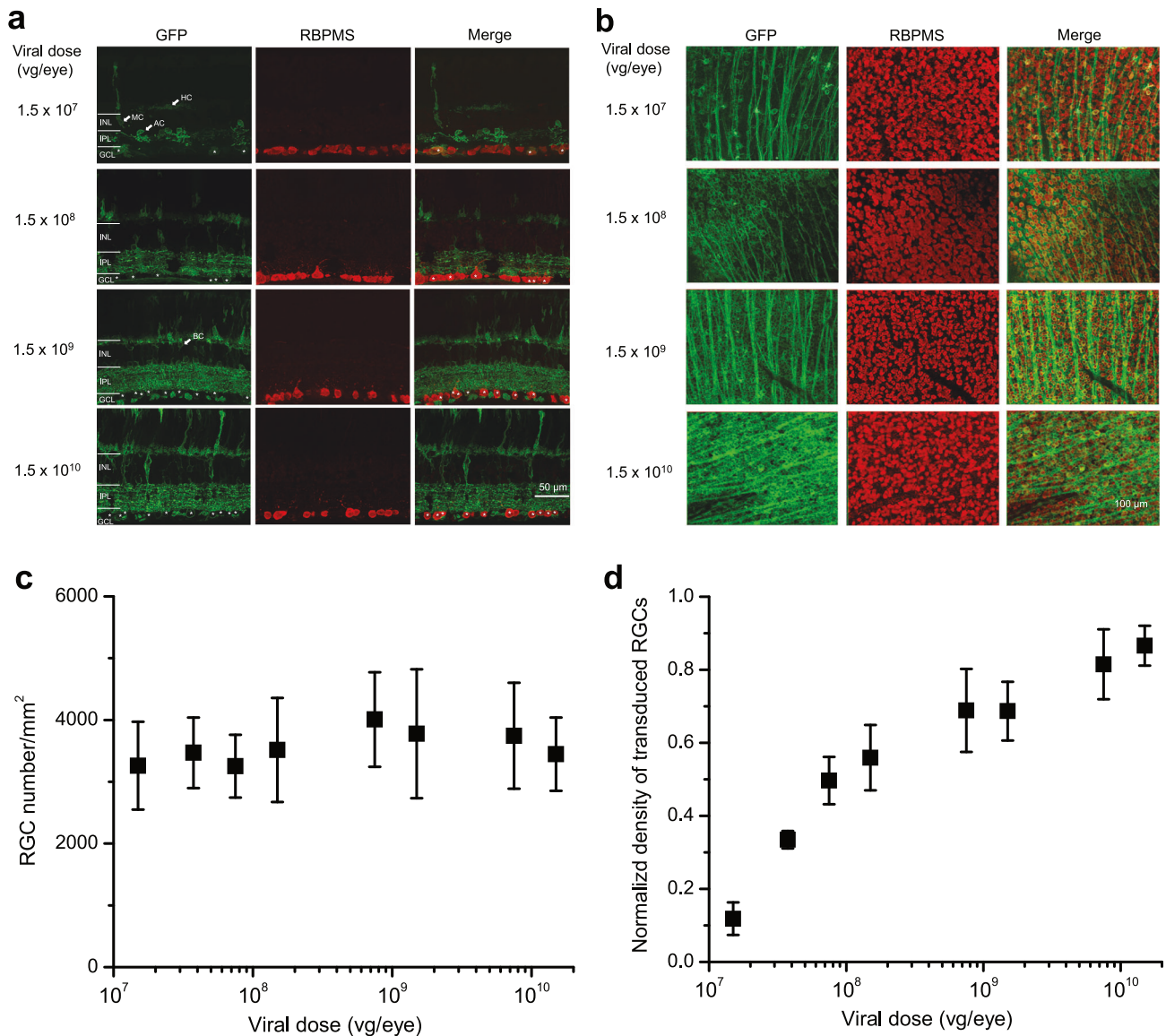
Fig. 3 Dose-dependent viral transduction efficiency. Representative immunofluorescence images of CoChR-3M-GFP in vertical retinal slices (**a**) and whole mounts (**b**) from treated TKO mice. Viral transduced RGCs were determined by GFP labeling. RGCs were labeled with an antibody against RBPMS, an RGC-specific marker. GFP and RBPMS co-labeled RGCs in retinal slices are marked with asterisks (*). **c** The relationship of RGC density and viral vector dose. RGC densities among all the treated groups are not statistically different ($p > 0.05$; one-way ANOVA). **d** The relationship between viral vector dose and the normalized density of transduced RGCs. The data are presented as means ± SD ($n = 4$ retinas in each dose group). Abbreviations: amacrine cell (AC); horizontal cell (HC); bipolar cell (BC); Müller cell (MC); inner nuclear layer (INL); inner plexiform layer (IPL); ganglion cell layer (GCL).

from the retinas injected with four different viral doses, from 1.5×10^7 to 1.5×10^{10} vg/eye. Viral transduced cells were labeled with an antibody against GFP (green). The specificity of the GFP antibody was confirmed in non-transduced retinas (data not shown). RGCs were labeled with an antibody against RBPMS (red), which is a specific marker for RGCs. As previously reported [3, 16, 34], CoChR-3M-GFP was predominantly expressed in RGCs, illustrated by the co-labeling with RBPMS (Fig. 3a, b). In addition, it was detected in other retinal cells, such as Müller cells, amacrine cells, horizontal cells, and, possibly, bipolar cells based on their localization and morphology (Fig. 3a).

We next examined the viral transduction efficiency in RGCs by immunostaining of retinal whole mounts. Transduced RGCs were identified by the co-labeling of GFP and RBPMS. First, RGC density based on RBPMS labeling was not significantly different among mice treated with different viral doses (Fig. 3c). On the other hand,

viral transduction efficiency, shown as the ratio of transduced RGCs to total RGCs, increased following the increase of viral dose (Fig. 3d). Specifically, about 12%, 56%, 69%, and 87% of RGCs were respectively transduced at the viral dose of 1.5×10^7, 1.5×10^8, 7.5×10^8, and 1.5×10^{10} vg/eye.

Protein expression of CoChR-3M-GFP

We also assessed the viral dose-dependent protein expression of CoChR-3M-GFP in the whole retina by Western blot assay using an antibody against GFP. For this assay, four retinas in each viral dose group were homogenized. A representative Western blot image is shown (Fig. 4a). The relationship between viral dose and the relative ECL fluorescence intensity of CoChR-3M-GFP after normalization to the ECL fluorescence intensity of β-actin (mean ± SD; from three experiments) was measured (Fig. 4b). The protein expression of CoChR-3M-GFP increased with viral dose at relatively
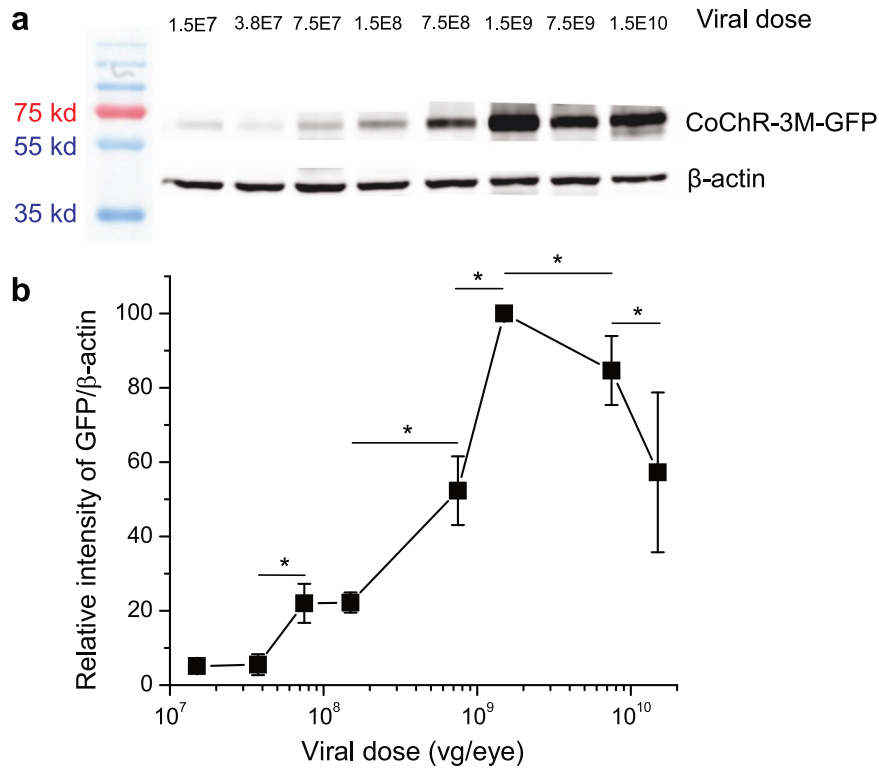
Fig. 4 Dose-dependent CoChR-3M-GFP protein expression by Western blot assay. a Representative Western blot images of CoChR-3M-GFP protein bands from whole retinas, labeled using an antibody against GFP. β-actin served as control. **b** The relative ECL fluorescence intensity of CoChR-3M-GFP after normalization by the ECL fluorescence intensity of β-actin. Four retinas were used for each viral dose group. Data are presented as means ± SD from three experiments.

low doses, peaked at the dose of ~1.5×10^9 vg/eye, then decreased with further increase of viral dose.

Assessment of gliosis and inflammation

Lastly, we assessed viral dose-dependent gliosis and inflammatory responses by immunostaining. Vertical retinal slices transduced with different viral doses were stained with an anti-GFAP antibody, a marker of retinal gliosis, and an anti-Iba1 antibody, a maker of microglia activation (Fig. 5a, b). Untreated TKO retinas served as controls. The quantitative results revealed similar dose-dependent patterns in immunoreactivity to GFAP and Iba1 (Fig. 5c, d). Specifically, the immunoreactivity is not significantly different from non-treated control retinas at viral doses up to 1.5×10^8 vg/eye but shows a significant increase at 1.5×10^9 vg/eye and a marked increase at 1.5×10^{10} vg/eye.

DISCUSSION

Based on our knowledge, this is the first study to examine AAV dose-dependent expression of optogenetic tools in RGCs based on the assessment of functional efficacy. Our results show both light sensitivity and visual acuity to be viral-dose-dependent. The light sensitivity rapidly increased, achieving ~50-fold difference, from the dose of 1.5×10^7 to 1.5×10^8 vg/eye, then approached a plateau at the dose of 7.5×10^8 vg/eye, with values not statistically different for higher doses. This pattern is largely consistent with the visual acuity assessment. First, at a viral dose of < 1.5×10^8 vg/eye, OMR was not observed, so that visual acuity could not be measured. As a note here, the failure to elicit OMR in TKO mice treated with these low doses is due to the fact that the light intensity required to elicit OMR exceeds the intensity of the OptoDrum system which is ~30 μW/cm^2 as indicated by the dashed line in Fig. 1b. On the other hand, visual acuity was observed in all TKO mice treated with viral doses ≥ 1.5×10^8, but

the values were not statistically different. Together, these results indicate that, for functional efficacy, a saturated viral dose occurred between 1.5×10^8 and 7.5×10^8 vg/eye.

As would be expected, our results show that the transduction efficiency of RGCs is also dose-dependent, increasing following the increase of viral dose. However, unlike the efficacy, the density of transduced RGCs did not plateau at the high tested doses. For example, about 56% and 69% of RGCs were transduced at viral doses of 1.5×10^8 and 7.5×10^8 vg/eye, respectively, and ~87% of RGCs were transduced at the viral dose of 1.5×10^{10} vg/eye. Interestingly, despite the proportion of transduced RGCs being markedly increased, light sensitivity and visual acuity did not significantly differ among animal groups receiving these viral doses. This might suggest that maximal functional efficacy occurs with the transduction of about two-thirds of RGCs. However, since there are more than 20 different types of RGCs, with each processing distinct visual information [35], it remains unknown whether functional efficacy is related to the transduction of particular types of RGCs. In addition, other retinal neurons, especially amacrine cells, were also transduced in this study and in previous reports [3, 34]; these cells may also contribute to functional efficacy.

In this study, we also assessed the protein of CoChR-3M-GFP by Western blot using whole retinal tissues. Interestingly, the viral dose and transgene protein expression exhibited an inverse V-shape relationship, with peak protein expression occurring at the viral dose of ~1.5×10^9 vg/eye. With further increase of dose, protein expression decreased. Since the overall density of RGCs was not found to be reduced at high doses, the decrease of protein expression is unlikely attributable to loss of RGCs, but rather suppression of the protein expression. This suppression may be caused by AAV-associated immune responses and associated adverse reactions exacerbated at high viral load. However, it is also possible that the suppression is caused by
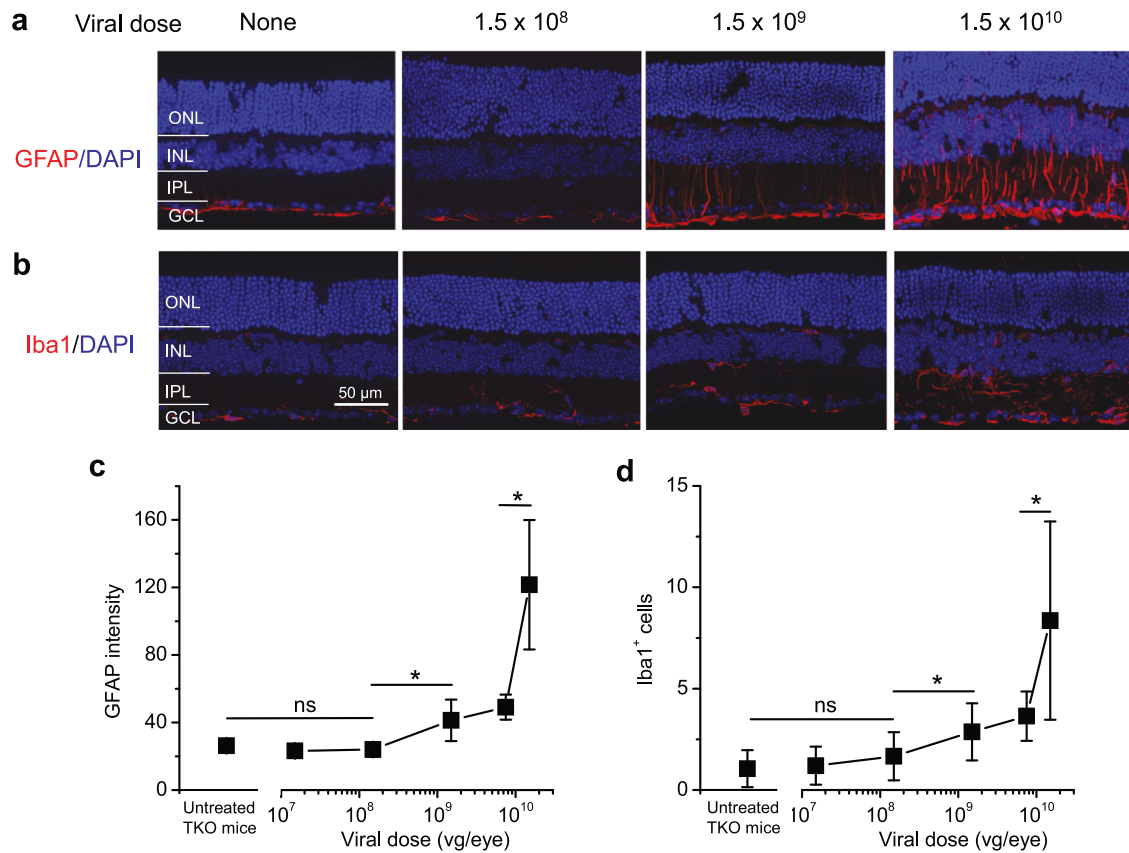
Fig. 5 Dose-dependent retinal gliosis and inflammation. Representative immunofluorescence images of vertical retinal slices showing GFAP (**a**) and Iba1 (**b**) immunoreactivity (in red) in untreated TKO mice and AAV-injected TKO groups. Cell nuclei were stained with DAPI (in blue). Relationship of GFAP fluorescence intensity (**c**) and Iba1 positive cells (**d**) to viral vector dose. All data are shown as mean ± SD ($n = 12$ images taken from six retinal slices in each dose group). For both GFAP and Iba1 immunoreactivity, the values for the groups with viral dose $\leq 1.5 \times 10^8$ vg/eye are not significantly different (ns) from the untreated control group ($p > 0.05$; one-way ANOVA). Asterisk (*) indicates the values between the groups are significantly different ($p < 0.05$; one-way ANOVA).

transgene overexpression-related cellular stress and/or injuries. A toxic effect of AAV-mediated GFP overexpression was previously reported [36]. Although the mechanism remains unknown, the observed decrease in transgene protein expression may in part explain the pattern of plateaued functional efficacy at higher doses. In addition, it is possible the plateaued efficacy is attributable to compromised RGC function and/or health due to transgene overexpression at high viral doses.

Although the retina is an immune privileged tissue, AAV vector- or transgene-triggered immune responses and associated adverse reactions particularly at high doses still pose a major concern in the development of retinal gene therapy [28, 29]. Indeed, in this study, our results revealed a viral-dose dependent increase of gliosis and inflammatory responses. Specifically, a significant increase of both GFAP and Iba1 immunoreactivity was observed at the dose of 1.5×10^9 vg/eye and a marked increase at the dose of 1.5×10^{19} vg/eye. As an important note, our results indicate that a maximal functional efficacy is reached before evoking a significant increase of retinal gliosis and inflammatory responses.

As a key finding of this study, our results suggest a capped or optimal viral dose near the medial of 10^8 vg for achieving maximal functional efficacy while largely avoiding gliosis and inflammatory responses in the mouse model, which provides valuable insights into dose design in clinical studies. Translating this to human studies, however, requires consideration of the differences between mice and humans. First, there is an up to ~1000× difference in vitreous volume between mice and humans (5 µL vs 4.5–5.0 mL) [37, 38]. Accordingly, to achieve the same viral titer in the vitreous humor of humans, the corresponding optimal viral

dose would be around 10^{11} vg/eye at least. Second, AAV transduction efficiency in mice is largely homogeneous through the retina, while that in humans is heterogeneous, as has been reported in non-human primates (NHPs) [39–41]. Specifically, in NHPs, high transduction occurs in the parafoveal and far peripheral retinal regions. In addition, unlike in humans, mouse retinas lack fovea. Furthermore, RGC subtypes vary between species. More than 40 distinct types have been identified in mice, comparing to 20 different types in humans [42, 43]. In particular, the majority of RGCs in humans are midget cells. It remains to be determined how these differences affect the dose and efficacy relationship.

DATA AVAILABILITY
The datasets generated during and/or analyzed during the current study are available from the corresponding author on reasonable request.

REFERENCES
1. Hartong DT, Berson EL, Dryja TP. Retinitis pigmentosa. Lancet. 2006;368:1795–809.
2. de Jong PT. Age-related macular degeneration. N Engl J Med. 2006;355:1474–85.
3. Bi A, Cui J, Ma YP, Olshevskaya E, Pu M, Dizhoor AM, et al. Ectopic expression of a microbial-type rhodopsin restores visual responses in mice with photoreceptor degeneration. Neuron. 2006;50:23–33.
4. Pan Z-H, Lu Q, Bi A, Dizhoor AM, Abrams GW. Optogenetic approaches to restoring vision. Annu Rev Vis Sci. 2015;1:185–210.
5. Simunovic MP, Shen W, Lin JY, Protti A, Lisowski L, Gillies MC. Optogenetic approaches to vision restoration. Exp Eye Res. 2019;178:15–26.

6. McClements ME, Staurenghi F, MacLaren RE, Cehajic-Kapetanovic J. Optogenetic gene therapy for the degenerate retina: recent advances. Front Neurosci. 2020;14:570909.

7. Sakai D, Tomita H, Maeda A. Optogenetic therapy for visual restoration. Int J Mol Sci. 2022;23:15041.

8. Sahel JA, Boulanger-Scemama E, Pagot C, Arleo A, Galluppi F, Martel JN, et al. Partial recovery of visual function in a blind patient after optogenetic therapy. Nat Med. 2021;27:1223–9.

9. Surace EM, Auricchio A. Versatility of AAV vectors for retinal gene transfer. Vision Res. 2008;48:353–9.

10. Tomita H, Sugano E, Yawo H, Ishizuka T, Isago H, Narikawa S, et al. Restoration of visual response in aged dystrophic RCS rats using AAV-mediated channelopsin-2 gene transfer. Investig Ophthalmol Vis Sci. 2007;48:3821–6.

11. Lin B, Koizumi A, Tanaka N, Panda S, Masland RH. Restoration of visual function in retinal degeneration mice by ectopic expression of melanopsin. Proc Natl Acad Sci USA. 2008;105:16009–14.

12. Nirenberg S, Pandarinath C. Retinal prosthetic strategy with the capacity to restore normal vision. Proc Natl Acad Sci USA. 2012;109:15012–7.

13. Sengupta A, Chaffiol A, Macé E, Caplette R, Desrosiers M, Lampic M, et al. Red-shifted channelrhodopsin stimulation restores light responses in blind mice, macaque retina, and human retina. EMBO Mol Med. 2016;8:1248–64.

14. Chaffiol A, Caplette R, Jaillard C, Brazhnikova E, Desrosiers M, Dubus E, et al. A new promoter allows optogenetic vision restoration with enhanced sensitivity in macaque retina. Mol Ther. 2017;25:2546–60.

15. Berry MH, Holt A, Salari A, Veit J, Visel M, Levitz J, et al. Restoration of high-sensitivity and adapting vision with a cone opsin. Nat Commun. 2019;10:1221.

16. Ganjawala TH, Lu Q, Fenner MD, Abrams GW, Pan Z-H. Improved CoChR variants restore visual acuity and contrast sensitivity in a mouse model of blindness under ambient light conditions. Mol Ther. 2019;27:1195–205.

17. Watanabe Y, Sugano E, Tabata K, Hatakeyama A, Sakajiri T, Fukuda T, et al. Development of an optogenetic gene sensitive to daylight and its implications in vision restoration. NPJ Regen Med. 2021;6:64.

18. Gauvain G, Akolkar H, Chaffiol A, Arcizet F, Khoei MA, Desrosiers M, et al. Optogenetic therapy: high spatiotemporal resolution and pattern discrimination compatible with vision restoration in non-human primates. Commun Biol. 2021;4:125.

19. Lagali PS, Balya D, Awatramani GB, Münch TA, Kim DS, Busskamp V, et al. Light-activated channels targeted to ON bipolar cells restore visual function in retinal degeneration. Nat Neurosci. 2008;11:667–75.

20. Doroudchi MM, Greenberg KP, Liu J, Silka KA, Boyden ES, Lockridge JA, et al. Virally delivered channelrhodopsin-2 safely and effectively restores visual function in multiple mouse models of blindness. Mol Ther. 2011;19:1220–9.

21. Busskamp V, Duebel J, Balya D, Fradot M, Viney TJ, Siegert S, et al. Genetic reactivation of cone photoreceptors restores visual responses in retinitis pigmentosa. Science. 2010;329:413–7.

22. Marc RE, Jones BW, Watt CB, Strettoi E. Neural remodeling in retinal degeneration. Prog Retin Eye Res. 2003;22:607–55.

23. Mazzoni F, Novelli E, Strettoi E. Retinal ganglion cells survive and maintain normal dendritic morphology in a mouse model of inherited photoreceptor degeneration. J Neurosci. 2008;28:14282–92.

24. Damiani D, Novelli E, Mazzoni F, Strettoi E. Undersized dendritic arborizations in retinal ganglion cells of the rd1 mutant mouse: a paradigm of early onset photoreceptor degeneration. J Comp Neurol. 2012;520:1406–23.

25. Kleinlogel S, Feldbauer K, Dempski RE, Fotis H, Wood PG, Bamann C, et al. Ultra light-sensitive and fast neuronal activation with the Ca^{2+}-permeable channelrhodopsin CatCh. Nat Neurosci. 2011;14:513–8.

26. Lu Q, Ganjawala TH, Hattar S, Abrams GW, Pan Z-H. A Robust optomotor assay for assessing the efficacy of optogenetic tools for vision restoration. Invest Ophthalmol Vis Sci. 2018;59:1288–94.

27. Hattar S, Lucas RJ, Mrosovsky N, Thompson S, Douglas RH, Hankins MW, et al. Melanopsin and rod-cone photoreceptive systems account for all major accessory visual functions in mice. Nature. 2003;424:76–81.

28. Drag S, Dotiwala F, Upadhyay AK. Gene therapy for retinal degenerative diseases: progress, challenges, and future directions. Investig Ophthalmol Vis Sci. 2023;64:39.

29. Hildegund CJ, Ertl HCJ. Immunogenicity and toxicity of AAV gene therapy. Front Immunol. 2022;13:975803.

30. Dalkara D, Byrne LC, Klimczak RR, Visel M, Yin L, Merigan WH, et al. In vivo-directed evolution of a new adeno-associated virus for therapeutic outer retinal gene delivery from the vitreous. Sci Transl Med. 2013;5:189ra76.

31. Petrs-Silva H, Dinculescu A, Li Q, Min SH, Chiodo V, Pang JJ, et al. High-efficiency transduction of the mouse retina by tyrosine-mutant AAV serotype vectors. Mol Ther. 2009;17:463–71.

32. Ecker JL, Dumitrescu ON, Wong KY, Alam NM, Chen S-K, LeGates T, et al. Melanopsin expressing retinal ganglion-cell photoreceptors: cellular diversity and role in pattern vision. Neuron. 2010;67:49–60.

33. Benkner B, Mutter M, Ecke G, Münch TA. Characterizing visual performance in mice: an objective and automated system based on the optokinetic reflex. Behav Neurosci. 2013;127:788–96.

34. Ivanova E, Pan Z-H. Evaluation of virus mediated long-term expression of channelrhodopsin-2 in the mouse retina. Mol Vision. 2009;15:1680–9.

35. Sanes JR, Masland RH. The types of retinal ganglion cells: current status and implications for neuronal classification. Annu Rev Neurosci. 2015;38:221–46.

36. Khabou H, Cordeau C, Pacot L, Fisson S, Dalkara D. Dosage thresholds and influence of transgene cassette in adeno-associated virus–related toxicity. Hum Gene Ther. 2018;29:1235–41.

37. Sebag J, Balazs EA. Morphology and ultrastructure of human vitreous fibers. Investig Ophthalmol Vis Sci. 1989;30:1867–71.

38. Azhdam AM, Goldberg RA, Ugradar S. In vivo measurement of the human vitreous chamber volume using computed tomography imaging of 100 eyes. Transl Vis Sci Technol. 2020;9:2.

39. Ivanova E, Hwang G-S, Pan Z-H, Troilo D. Evaluation of AAV-mediated expression of Chop2-GFP in the marmoset retina. Investig Ophthalmol Vis Sci. 2010;51:5288–96.

40. Yin L, Greenberg K, Hunter JJ, Dalkara D, Kolstad KD, Masella BD, et al. Intravitreal injection of AAV2 transduces macaque inner retina. Investig Ophthalmol Vis Sci. 2011;52:2775–83.

41. Wang W, Nan Y, Pan Z-H, Pu M. Morphological evaluation of retinal ganglion cells expressing the L132C/T159C ChR2 mutant transgene in young adult cynomolgus monkeys. Sci China Life Sci. 2017;60:1157–67.

42. Rheaume BA, Jereen A, Bolisetty M, Sajid MS, Yang Y, Renna K, et al. Single cell transcriptome profiling of retinal ganglion cells identifies cellular subtypes. Nat Commun. 2018;9:2759.

43. Yan W, Peng YR, van Zyl T, Regev A, Shekhar K, Juric D, et al. Cell atlas of the human fovea and peripheral retina. Sci Rep. 2020;10:9802.

ACKNOWLEDGEMENTS

AUTHOR CONTRIBUTIONS
QL and ZHP designed the experiments. QL, AW, and ZHP performed experiments and analyzed data; QL and ZHP wrote paper.

COMPETING INTERESTS
ZHP and QL are inventors of patents related to optogenetic vision restoration. ZHP serves as a scientific advisor and QL serves as a consultant to Ray Therapeutics, Inc. AW declares no competing interests.

ETHICAL APPROVAL
All animal studies were approved by the Institutional Animal Care and Use Committee.

ADDITIONAL INFORMATION
Correspondence and requests for materials should be addressed to Zhuo-Hua Pan.

Reprints and permission information is available at http://www.nature.com/reprints

Publisher's note Springer Nature remains neutral with regard to jurisdictional claims in published maps and institutional affiliations.

8